

# Quantum reflection times and space shifts for Casimir–van der Waals potential tails

Alexander Jurisch and Harald Friedrich

*Physik-Department, Technische Universität München, 85747 Garching bei München, Germany*

(Received 7 May 2004; published 23 September 2004)

When cold atoms approach a surface, they can be quantum reflected by quantal regions in the tail of the atom-surface potential. We study the phase of the reflection amplitude for Casimir–van der Waals potential tails, depending on the critical parameter  $\rho = \rho(C_3, C_4)$ , which describes the relative importance of the  $-C_3/r^3$  and  $-C_4/r^4$  parts of the potential. The phase is related to observable kinematic quantities, the space and time shifts, the reflected atom experiences. We study three different models for the shape of the potential between the asymptotic limits and observe that the phases are more sensitive to the potential shape than the quantum reflection probabilities. At threshold, there are always time delays in comparison to the free movement. This is in contrast to the classical movement, which shows time gains. Further above threshold, the quantum reflected atom experiences a time gain relative to free motion, but this time gain is generally smaller than that of the classical particle.

DOI: 10.1103/PhysRevA.70.032711

PACS number(s): 34.10.+x, 34.50.Dy, 03.65.–w, 03.75.Be

## I. INTRODUCTION

Quantum reflection happens to a particle moving through a classically allowed region without reaching a classical turning point—it is a pure quantum effect. It is most intense for particles moving with small velocity and is thus connected to the large and rapidly growing field of research with ultracold atoms. The asymptotic free motion of such particles is classical, but the motion becomes increasingly quantum mechanical, when the potential becomes non-negligible. When the potential tail falls off faster than  $-1/r^2$ , the motion again becomes classical at *small* distances, which may still be large compared with a few atomic units, where the interaction structure is more complicated. The inner classical region and the asymptotic free classical region are separated by the *quantal* region, where the motion is nonclassical. This region lies typically hundreds or thousands of atomic units distant from the inner potential region, and the interactions there are well described by attractive local potential tails. In this quantal region, quantum reflection occurs. To treat the reflection problem, it is thus sufficient to know the potential tail, because all inner effects, e.g., inelastic reactions or sticking, do not come into play.

For large distances, a stationary solution of the Schrödinger equation at energy  $\hbar^2 k^2/2M$  has the form

$$\psi(r) \sim \frac{1}{\sqrt{\hbar k}} \{ \exp[-ikr] + R(k) \exp[ikr] \}, \quad (1)$$

where  $R$  is the reflection amplitude  $R(k) = |R(k)| \exp[i\phi(k)]$ . The quantum reflection probability  $|R(k)|^2$  approaches unity at threshold and is thus always non-negligible, when the velocities of incident particles are small enough. It has been subject to intense recent research, theoretically [1–6], and experimentally [7,8]. Its behavior at threshold for potentials falling off faster than  $-1/r^2$  is universal and given by

$$\lim_{k \rightarrow 0} |R(k)| \sim 1 - 2bk = \exp[-2bk] + O(k^2). \quad (2)$$

The parameter  $b$ , the *threshold length*, is a characteristic

property of the potential tail and also determines properties of bound states just below threshold. For an exhaustive review on this topic, see [9]. In a recent Letter [10], we investigated the behavior of a wave packet being quantum reflected at atomic potential tails of type

$$V(r) = -\frac{C_\alpha}{r^\alpha} = -\frac{\hbar^2}{2M} \frac{(\beta_\alpha)^{\alpha-2}}{r^\alpha}, \quad \alpha > 2. \quad (3)$$

What makes the phase of the quantum reflection amplitude an interesting quantity is its close relation to observable kinematical quantities, namely, the space and time shifts the wave packet undergoes during the reflection process. For a wave packet with a narrow momentum distribution peaked around  $\hbar k_0$ , the space shift  $\Delta r$  and the time shift  $\Delta t$  are given by [11]

$$\Delta r = -\left. \frac{1}{2} \frac{d\phi(k)}{dk} \right|_{k=k_0},$$

$$\Delta t = \frac{2\Delta r}{v_0} = -\left. \frac{M}{\hbar k_0} \frac{d\phi(k)}{dk} \right|_{k=k_0} = -\left. \hbar \frac{d\phi(E)}{dE} \right|_{E=\hbar^2 k_0^2/2M}. \quad (4)$$

The space and time shifts (time gain for  $\Delta t > 0$  or loss for  $\Delta t < 0$  during the reflection process) are to be seen in comparison to a free moving wave packet. We want to emphasize that the space shift the reflected atom experiences is an apparent quantity. Its apparent character becomes clear by the schematic picture of the quantum reflection process shown in Fig. 1. The reflection occurs in the quantal region around the point  $r_E$ , which is defined by

$$E = \frac{\hbar^2 k^2}{2M} = |V(r_E)|, \quad (5)$$

where the absolute value of the potential equals the (asymptotic) kinetic energy [3,12]. The time evolution of the reflected wave packet corresponds to a reflection of a free wave at the point  $r = \Delta r$  rather than  $r = 0$ , where it would be

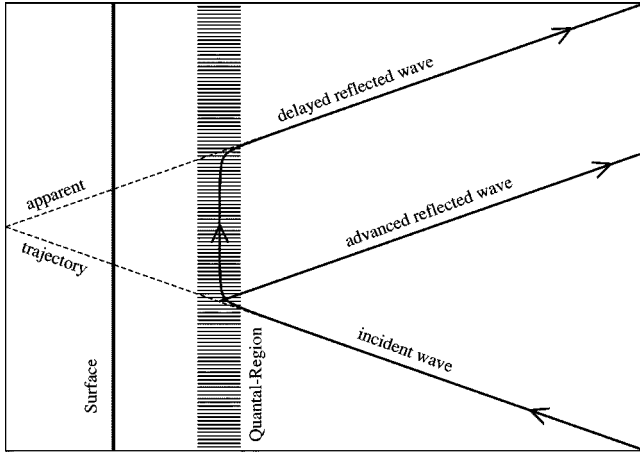


FIG. 1. Schematic illustration of the quantum reflection process. An advanced reflected wave travels as a free wave reflected in front of the surface. When the quantum reflection process involves a time delay, the reflected wave travels as a free wave reflected behind the surface.

reflected without potential. When the sign of  $\Delta r$  is positive, the quantum reflected particle appears to be reflected in front of the surface and experiences a time gain in comparison to the free particle. But when the sign of  $\Delta r$  is negative, the quantum reflected particle behaves as if it would enter the region behind the surface. The negative sign corresponds to a time delay relative to the free moving particle. While the movement parallel to the surface is not affected by quantum reflection, the particle continues its free movement parallel to the surface, but the perpendicular motion is delayed in the quantal region so that the reflected wave appears to have been reflected at  $\Delta r < 0$ , as illustrated in Fig. 1. The general threshold law for the phase of the reflection amplitude is [10]

$$\lim_{k \rightarrow 0} \phi(k) \sim \pi - 2\bar{a}k, \quad \lim_{k_0 \rightarrow 0} \Delta r = \bar{a}, \quad (6)$$

where  $\bar{a}$  is the mean scattering length of the potential tail. This quantity is determined only by the potential tail [13] and should not be confused with the (total) scattering length  $a$ . For homogeneous potentials and high energies, the phase behaves as

$$\lim_{k \rightarrow \infty} \phi(k) \propto -k^{1-2/\alpha}. \quad (7)$$

In this paper, we focus on Casimir–van der Waals potential types, which give a realistic description of the atom–surface interaction. Their structure can be understood as a mixture of two potential tails, the van der Waals tail, proportional to  $-1/r^3$ , and the highly retarded or Casimir-Polder tail, proportional to  $-1/r^4$ . As was shown in [10], the behavior of these tails is as different as can be. In the case of a pure  $-1/r^3$  interaction, the space and time shift tend to minus infinity for small incoming velocities, which means that the motion is strongly delayed. In contrast, in a pure  $-1/r^4$  potential, the space shift tends to zero and the time shift remains finite for small incoming velocities. Thus we have no significant difference from a free motion at threshold. In the present paper, we investigate how the presence of both pow-

ers changes the kinematic behavior of a quantum reflected particle.

Our paper is organized as follows. In Sec. II we outline the Casimir-Polder theory and give scaling arguments for the relative importance of the two intrinsic length scales to be found in the Casimir–van der Waals problem. In Sec. III, which is the main section of our article, we examine the phase of the quantum reflection amplitude and the space and time shifts for three model potentials in detail, focusing especially on the transition region from one dominant scale to the other. In Sec. IV we conclude by summarizing our results.

## II. GENERAL ASPECTS OF CASIMIR–VAN DER WAALS INTERACTION

The Casimir–van der Waals potential describing the interaction between a spherically symmetric ground state atom and a perfectly conducting surface can be calculated by knowledge of the dynamical atomic dipole polarizability  $\alpha_d(i\omega)$  [14]. In atomic units it reads [15]

$$V_{\text{CvdW}}(r) = -\frac{1}{4\pi r^3} \int_0^\infty d\omega \alpha_d(i\omega) [1 + 2\alpha_{fs}\omega r + 2(\alpha_{fs}\omega r)^2] \exp[-2\alpha_{fs}\omega r],$$

$$\alpha_d(i\omega) = \sum_n 2(E_n - E_m) \frac{|\langle m | \sum_{j=1}^Z z_j | n \rangle|^2}{(E_n - E_m)^2 + \omega^2}. \quad (8)$$

$\alpha_{fs}$  is the fine-structure constant. The asymptotic behavior for small and large distances is given by the limits

$$\lim_{r \rightarrow 0} V_{\text{CvdW}}(r) \sim -\frac{C_3}{r^3} = -\frac{\hbar^2 \beta_3}{2M r^3},$$

$$\lim_{r \rightarrow \infty} V_{\text{CvdW}}(r) \sim -\frac{C_4}{r^4} = -\frac{\hbar^2 \beta_4^2}{2M r^4}, \quad (9)$$

and the strength parameters are

$$C_3 = \frac{1}{4\pi} \int_0^\infty \alpha_d(i\omega) d\omega, \quad C_4 = \frac{3}{8\pi\alpha_{fs}} \alpha_d(0). \quad (10)$$

When the interaction of polarizable atoms and a dielectric surface is considered, the above formulas become a little more complicated. The full interaction now is given by (see, e.g., [16,17])

$$V(r, \epsilon) = -\frac{\alpha_{fs}^3}{2\pi} \int_0^\infty d\omega \alpha_d(i\omega) \omega^3 \int_1^\infty dp \exp[-2\omega r p \alpha_{fs}] h(p, \epsilon),$$

$$h(p, \epsilon) = \frac{\sqrt{\epsilon - 1 + p^2} - p}{\sqrt{\epsilon - 1 + p^2} + p} + (1 - 2p^2) \frac{\sqrt{\epsilon - 1 + p^2} - \epsilon p}{\sqrt{\epsilon - 1 + p^2} + \epsilon p}. \quad (11)$$

Here  $\epsilon$  is the dielectric constant. From this, the strength parameters in the dielectric case follow as [16,18]

$$C_3(\epsilon) = \frac{\epsilon - 1}{\epsilon + 1} C_3(\infty), \quad C_4(\epsilon) = \frac{\epsilon - 1}{\epsilon + 1} \Phi(\epsilon) C_4(\infty), \quad (12)$$

where the characteristic function  $\Phi(\epsilon)$  is given by

$$\Phi(\epsilon) = \frac{\epsilon + 1}{2(\epsilon - 1)} \int_0^\infty dp \frac{h(p + 1, \epsilon)}{(p + 1)^4}. \quad (13)$$

The characteristic function  $\Phi(\epsilon)$  increases monotonically from  $\Phi(1) = 23/30$  to  $\Phi(\infty) = 1$ .

For homogeneous potentials (3), the Schrödinger equation depends not on  $E = \hbar^2 k^2 / 2M$  and  $\beta_\alpha$  independently, but only on  $(k\beta_\alpha)$ . In contrast, Casimir–van der Waals potentials contain two different quantum mechanical length scales  $\beta_3, \beta_4$ , which define an intrinsic energy-independent length  $l$  [3],

$$l = \frac{C_4}{C_3} = \frac{\beta_4^2}{\beta_3}. \quad (14)$$

The intrinsic length  $l$  allows us to define two dimensionless variables

$$x = \frac{r}{l}, \quad \kappa = kl. \quad (15)$$

A strength parameter  $K_0$  for the potential can be introduced in full generality as

$$\frac{\hbar^2 K_0^2}{2M} = \frac{C_3}{l^3} = \frac{C_4}{l^4} \Rightarrow K_0 = \frac{(\beta_3)^2}{(\beta_4)^3}, \quad (16)$$

allowing the Casimir–van der Waals potential to be written as

$$V_{\text{CvdW}}(r) = -\frac{\hbar^2 K_0^2}{2M} v\left(\frac{r}{l}\right). \quad (17)$$

The transformation of the Schrödinger equation for  $\psi = \psi(x = r/l)$  gives

$$\left[ \frac{d^2}{dx^2} + \kappa^2 + \rho^2 v(x) \right] \psi(x) = 0, \quad (18)$$

$$\rho = K_0 l = \frac{\beta_3}{\beta_4} = \frac{\sqrt{2M} C_3}{\hbar \sqrt{C_4}}.$$

The parameter  $\rho$  is the critical parameter of the system. When  $\rho < 1$ , the  $-1/r^3$  contribution is dominant for quantum reflection and retardation effects become negligible, whereas for  $\rho > 1$ , the  $-1/r^4$  contribution is dominant and the pure van der Waals interaction becomes less important.

If  $\rho(\infty)$  is the critical parameter for the Casimir–van der Waals interaction of a given atom with a perfectly conducting surface, then for a dielectric surface it is

$$\rho(\epsilon) = \rho(\infty) \frac{1}{\sqrt{\Phi(\epsilon)}} \sqrt{\frac{\epsilon - 1}{\epsilon + 1}}. \quad (19)$$

A dielectric surface shortens the two relevant length scales of the Casimir–van der Waals potential, and thus the  $\rho$  parameter also decreases. The two limiting cases are given by

$$\lim_{\epsilon \rightarrow \infty} \rho(\epsilon) = \rho(\infty), \quad \lim_{\epsilon \rightarrow 1} \rho(\epsilon) = 0. \quad (20)$$

### III. CALCULATION OF THE PHASE OF $R(k)$

In the following main section of our article, we discuss phases, and space- and time-shifts for Casimir–van der Waals-potentials. Since the exact shape of the potential is not known in general, we study three models suggested in the literature. The potential assumed by Shimizu [7] found its validation by fitting well the experimental quantum reflection data [7,8], and can be regarded as a simpler form of the rational approximation given by Friedrich, Jacoby, and Meister [3] and improved by Friedrich and Trost [9]. The rational approximation was derived by fitting the exact potential for a hydrogen atom, interacting with a conducting surface, given by Marinescu *et al.* [19]. Last, we investigated the behavior of a potential calculated by Feinberg and Sucher [20], and later Holstein [21], which we have adapted for our present purposes, and which we will refer to as the arctan formula. A detailed examination of the potentials now follows.

#### A. Model potentials

In terms of dimensionless variables  $x = r/l$ ,  $\rho = K_0 l$ , the potential used by Shimizu [7] is

$$V_S(x) = -\rho^2 \frac{1}{x^3(1+x)}. \quad (21)$$

It has the advantage of allowing analytical treatment of the threshold behavior of the phase of the quantum reflection amplitude. According to the above scaling laws, the wave function at threshold can be expressed in terms of Hankel functions [22]

$$\psi(x) = \sqrt{x(x+1)} H_1^{(1)} \left( 2\rho \sqrt{\frac{x+1}{x}} \right). \quad (22)$$

Its asymptotic expression,  $x \rightarrow \infty$ , follows readily as

$$\lim_{x \rightarrow \infty} \psi(x) \sim \psi_\infty(x), \quad \psi_\infty(x) \sim \rho H_0^{(1)}(2\rho) + x H_1^{(1)}(2\rho). \quad (23)$$

Matching the asymptotic wave function  $\psi_\infty(x)$  to asymptotic plane waves (1) in the limit  $kr = \kappa x \rightarrow 0$ , the reflection coefficient is found to be

$$R(\kappa) = -\frac{H_1^{(1)}(2\rho) + i\kappa\rho H_0^{(1)}(2\rho)}{H_1^{(1)}(2\rho) - i\kappa\rho H_0^{(1)}(2\rho)} \approx -1 - i2\kappa\rho \frac{H_0^{(1)}(2\rho)}{H_1^{(1)}(2\rho)}. \quad (24)$$

When decomposing the Hankel functions into Bessel and Neumann functions, the reflection coefficient can be expressed in real and imaginary parts:

$$R(\kappa) = -1 + 2\kappa \frac{1}{\pi[J_1^2(2\rho) + N_1^2(2\rho)]} - i2\kappa\rho \frac{J_0(2\rho)J_1(2\rho) + N_0(2\rho)N_1(2\rho)}{J_1^2(2\rho) + N_1^2(2\rho)}. \quad (25)$$

The second term, giving the threshold length, has already been derived in [3] by a different calculation. From the above expression, the phase at threshold follows as

$$\lim_{\kappa \rightarrow 0} \phi(\kappa) \sim \pi + 2\kappa\rho \frac{J_0(2\rho)J_1(2\rho) + N_0(2\rho)N_1(2\rho)}{J_1^2(2\rho) + N_1^2(2\rho)}. \quad (26)$$

According to the general threshold law for phases given in [10], Eq. (6), the potential, Eq. (21) has a negative mean scattering length

$$\bar{a}/l = -\rho \frac{J_0(2\rho)J_1(2\rho) + N_0(2\rho)N_1(2\rho)}{J_1^2(2\rho) + N_1^2(2\rho)}. \quad (27)$$

A rational approximation fitting the Casimir–van der Waals interaction for hydrogen and hydrogenlike atoms was first introduced in [3] and was brought into an improved form in [9],

$$V_{\text{RA}}(x) = -\rho^2 \frac{1 + \zeta x}{x^3(1 + x + \zeta x^2)}, \quad \zeta = 0.31608. \quad (28)$$

The arctan formula [20,21] is given by

$$V_{\text{arc}}(x) = -\rho^2 \frac{2}{\pi x^3} \arctan\left[\frac{\pi}{2x}\right]. \quad (29)$$

For the rational approximation and the arctan formula, analytical treatment is not even available for threshold behavior and we have to rely on numerical calculations only.

### B. Phases, space shifts, and time shifts

For a given shape of the atom-surface potential, the phases of the quantum reflection amplitudes we have calculated in this section are functions  $\phi = \phi(k, \beta_3, \beta_4)$ . Applying the scaling laws [see Eq. (18)], we find

$$\phi(k, \beta_3, \beta_4) = \phi\left(kl, \frac{\beta_3}{\beta_4}\right) = \phi(\kappa, \rho). \quad (30)$$

This can be seen easily by calculating the space shift

$$\frac{\Delta r}{l} = -\frac{1}{2l} \frac{d\phi(k, \beta_3, \beta_4)}{dk} = -\frac{1}{2} \frac{d\phi(\kappa, \rho)}{d\kappa}. \quad (31)$$

Every single value of  $\rho$  represents many possible combinations of  $\beta_3, \beta_4$ , although only few of these may be realized in nature. The phases and space shifts we have calculated are for values  $\rho=0.5, 1, 3$ . This parameter range covers the most interesting regions of the interaction, namely,  $\rho < 1$ , where the  $-1/r^3$  tail is dominant,  $\rho > 1$ , where the  $-1/r^4$  part is dominant, and  $\rho=1$ , where both parts of the interaction are of equal influence. Although we will always discuss the behavior of the time shifts too, we decided to plot just the space

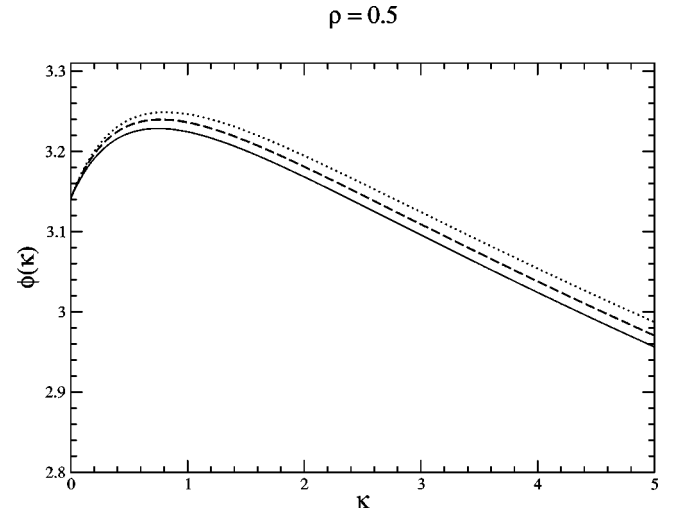


FIG. 2. Phases of the quantum reflection amplitude at  $\rho=0.5$ . Shimizu's potential (21) (full line), rational approximation (28) (dashed line), and arctan formula (29) (dotted line).

shifts. The time shifts always diverge to negative infinity at threshold, indicating strong time delays, but the space shifts remain finite there, and thus are easier to study.

Figures 2 and 3 show the phases and the space shifts for  $\rho=0.5$ . The phases show a similar behavior as was calculated for a pure van der Waals potential in [10]. They show a characteristic maximum, typical for a  $-1/r^3$  potential, which indicates the dominance of the van der Waals part of the interaction. The space shifts for small energies are negative until  $\kappa_0 \approx 0.8$ , meaning that quantum reflected atoms with  $\kappa_0$  smaller than approximately 0.8 are delayed in comparison to free moving atoms. For a pure  $-1/r^3$  potential the threshold behavior of the space shift is logarithmically divergent [10], but the space shift remains finite at threshold for a Casimir–van der Waals interaction, although the  $-1/r^3$  part is dominant for  $\rho=0.5$ , because the highly retarded tail  $-1/r^4$  is present for  $r \rightarrow \infty$ . Figures 4 and 5 show phases and space

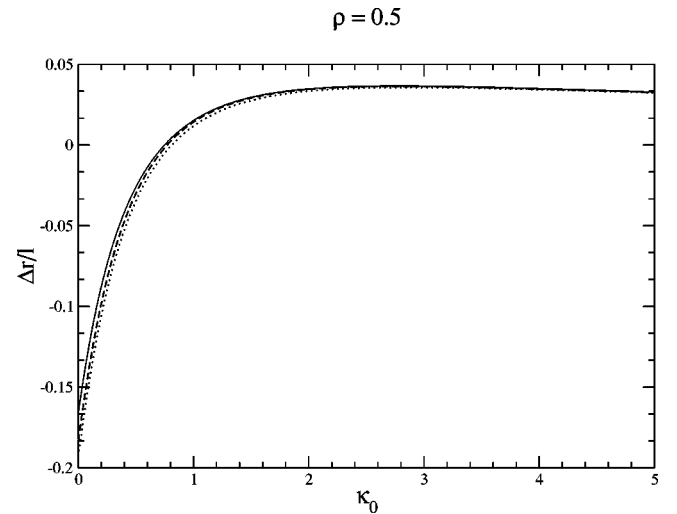


FIG. 3. Quantum space shifts at  $\rho=0.5$ . Shimizu's potential (21) (full line), rational approximation (28) (dashed line), and arctan formula (29) (dotted line).

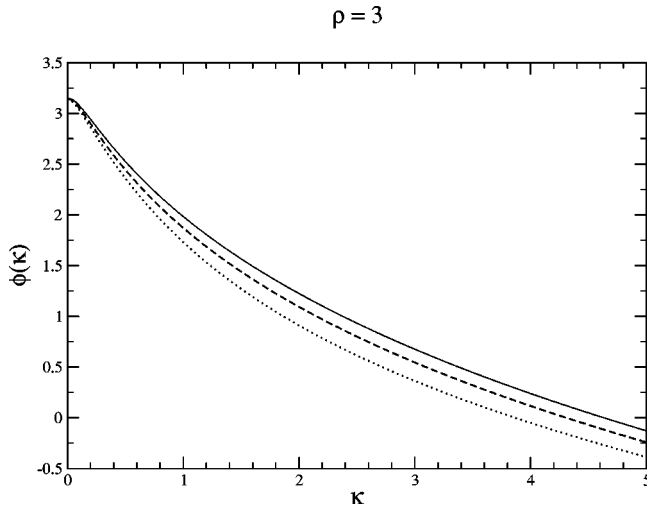


FIG. 4. Phases of the quantum reflection amplitude at  $\rho=3$ . Shimizu's potential (21) (full line), rational approximation (28) (dashed line), and arctan formula (29) (dotted line).

shifts for  $\rho=3$ , where the  $-1/r^4$  contribution dominates the reflection process up to quite high energies. The characteristic van der Waals maximum at threshold has almost disappeared and the region of negative space shifts has shrunk to energies  $\kappa_0 < 0.02$ . For larger energies, the shape of the phases shows a behavior very similar to a pure  $-1/r^4$  interaction, as was calculated in [10]. The relative dominance of the  $-1/r^4$  interaction favors time gains for the reflected atom. The tendency for time gains is largest for energies  $0.1 < \kappa_0 < 1$ , where the space shift shows its maximum. Figures 6 and 7 show phases and space shifts for  $\rho=1$ . We are now in the parameter range where both parts of the potential show comparable influences for quantum reflection. Again we find the characteristic van der Waals maximum in the threshold region, but it is already reduced and not as dominant as it was at  $\rho=0.5$ . For larger  $\kappa$  the phases fall off much faster, which already indicates similarity with the pure  $-1/r^4$

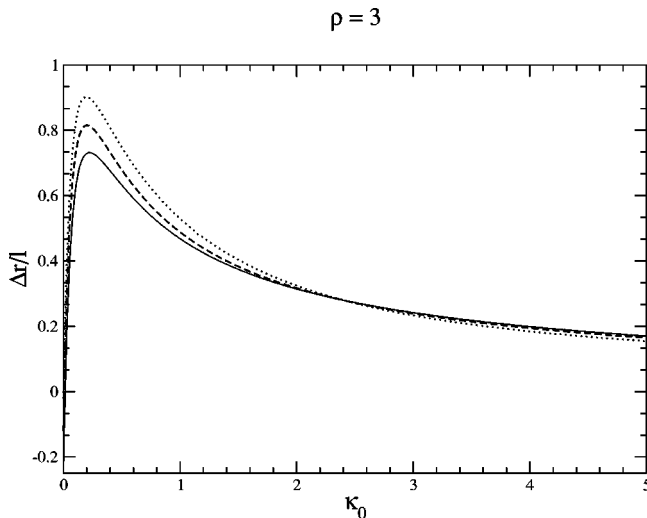


FIG. 5. Quantum space shifts at  $\rho=3$ . Shimizu's potential (21) (full line), rational approximation (28) (dashed line), and arctan formula (29) (dotted line).

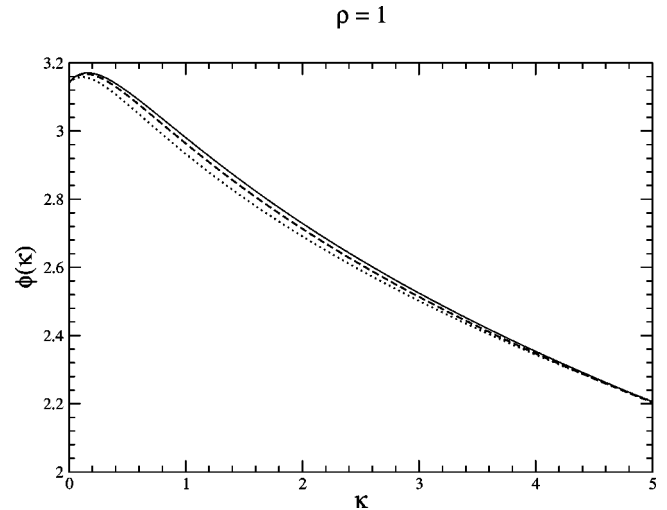


FIG. 6. Phases of the quantum reflection amplitude at  $\rho=1$ . Shimizu's potential (21) (full line), rational approximation (28) (dashed line), and arctan formula (29) (dotted line).

shape calculated in [10]. This behavior becomes clearer when we consider the space shifts. The space shift remains negative only for values  $\kappa_0 < 0.1$ . Thus, there is a time delay for a reflected atom only very close to threshold, whereas for  $\kappa_0 > 0.1$  there is already a time gain, compared to the free movement.

### C. Comparison to the classical motion

The classical time shift can be calculated by comparing a classical free motion with the classical motion in the potential. The time gain of the classical particle moving in the potential relative to the free particle is

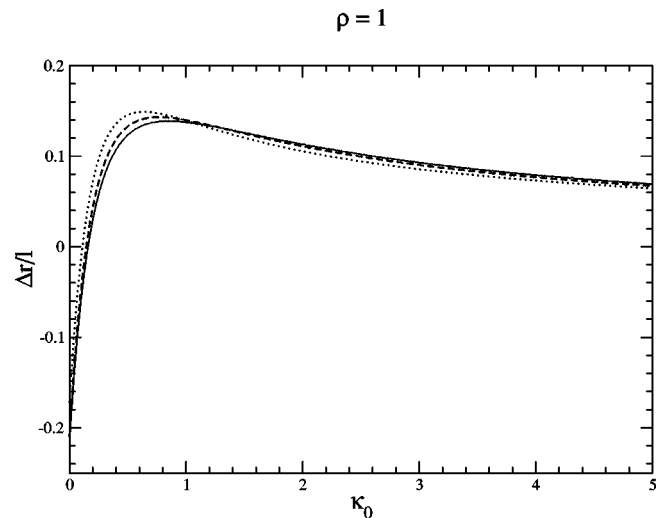


FIG. 7. Quantum space shifts at  $\rho=1$ . Shimizu's potential (21) (full line), rational approximation (28) (dashed line), and arctan formula (29) (dotted line).

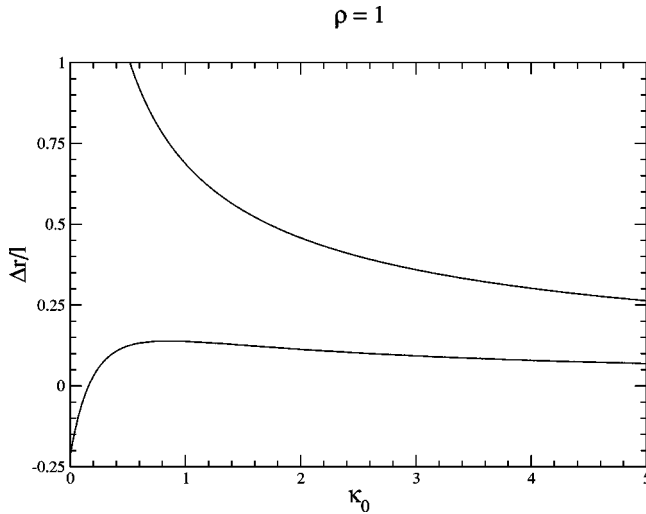


FIG. 8. Comparison between quantum space shift and classical space shift obtained with Shimizu's potential (21).

$$\begin{aligned} \Delta t_{\text{cl}} &= 2 \lim_{r \rightarrow \infty} \int_0^r \left( \frac{1}{v_0} - \frac{1}{|v(r')|} \right) dr' \\ &= 2M \int_0^\infty \left( \frac{1}{\hbar k_0} - \frac{1}{p(r)} \right) dr > 0. \end{aligned} \quad (32)$$

Applying scaling as above, this expression can be cast into the following suitable form:

$$\Delta t_{\text{cl}} = \frac{2M}{\hbar k_0} l \int_0^\infty dx \left( 1 - \frac{1}{\sqrt{1 + (\rho^2/\kappa_0^2)v(x)}} \right). \quad (33)$$

This integral cannot be calculated analytically for any of the model potentials. Abbreviating the integral as  $\tau$ ,

$$\Delta t_{\text{cl}} = \frac{2M}{\hbar k_0} l \tau \left( \frac{\rho}{\kappa_0} \right), \quad (34)$$

this corresponds to the classical space shift

$$\Delta r_{\text{cl}}/l = \tau \left( \frac{\rho}{\kappa_0} \right). \quad (35)$$

The classical space shift in units of  $l$  depends only on the ratio  $\rho/\kappa_0$ , as given by the function  $\tau(\rho/\kappa_0)$ . This is in contrast to our results found in [10], where the classical space shift is given by a simple power law. But in the Casimir–van der Waals interaction we have effectively a mixture of two powers  $\alpha=(3,4)$ , and thus the space shift cannot be described by a pure power law.

In Fig. 8, we plotted the quantum space shift and the classical space shift for Shimizu's potential for  $\rho=1$ . We observe that the quantum space shift is smaller than the classical one, which diverges to positive infinity at threshold. Near threshold, the classical particle experiences large time gains, whereas the quantum particle experiences a finite negative space shift, corresponding to large time delays relative to the free particle. We remind the reader that the threshold region of Casimir–van der Waals potentials is the anticlassical limit of the Schrödinger equation (see [9]). Thus we indeed would

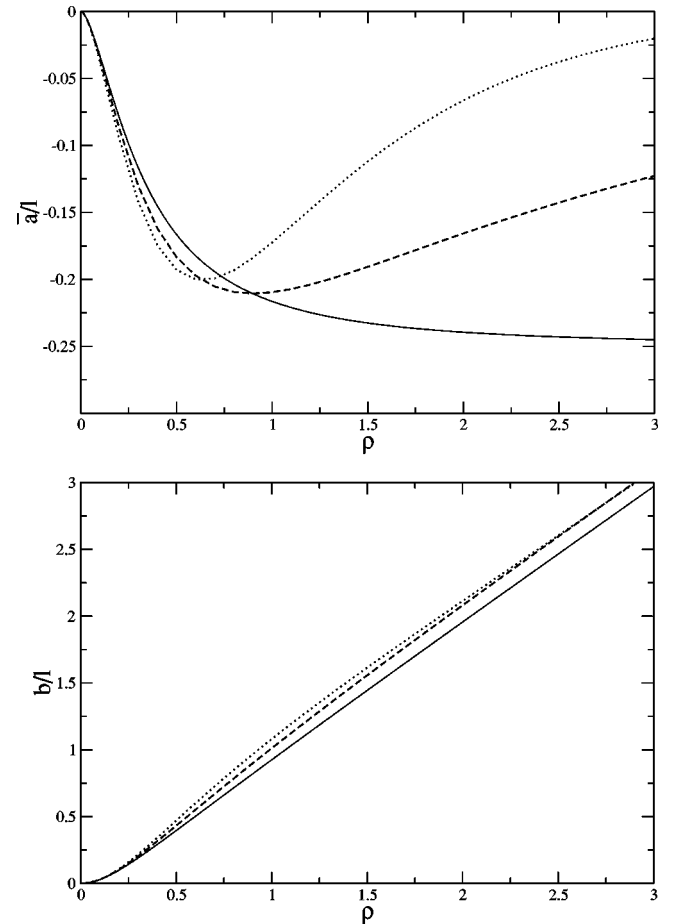


FIG. 9. Mean scattering length (above) and threshold length (below) as functions of  $\rho$ . Shimizu's potential (21) (full line), rational approximation (28) (dashed line), and arctan formula (29) (dotted line).

expect the most distinct differences between quantum and classical behavior to occur there. For large scaled momenta  $\kappa_0$ , the behavior becomes more and more classical, and a close examination of the curve shape indeed supports this conjecture. Generally, the results presented in [10] for homogeneous potentials, stating that the quantum space shift is always smaller than the classical one, indicating the quantum movement to be always slower than the classical one, is confirmed for Shimizu's potential. For the rational approximation (28) and the arctan formula (29), the qualitative behavior is the same.

#### D. The mean scattering length

The mean scattering length is an important quantity, because it determines the behavior of the phase of  $R(k)$  at threshold. Figure 9 shows  $\bar{a}/l$  for our model potentials as a function of  $\rho$ . For small  $\rho$ , their behavior is similar, but as  $\rho$  grows to unity and beyond, distinct differences between the model potentials arise. For Shimizu's potential,  $\bar{a}/l$  converges to a finite value  $-0.25$ , while the rational approximation and the arctan formula show a tendency to zero, as  $\rho$  grows beyond all bounds. It is interesting to compare the

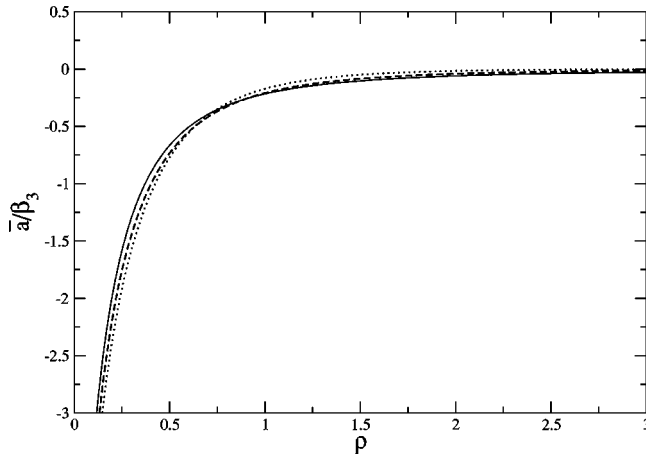


FIG. 10. Mean scattering length on  $\beta_3$  scale. Shimizu's potential (21) (full line), rational approximation (28) (dashed line), and arctan formula (29) (dotted line).

behavior of the mean scattering length  $\bar{a}/l$  with the behavior of the threshold length  $b/l$ , which determines the near threshold behavior of the reflection probability [see Eq. (2)]. We clearly see that the behavior of the phases and thus the behavior of the space shifts and mean scattering lengths are much more sensitive to the shape of the potential than is the behavior of the reflection probability. In Figs. 10 and 11, we plotted the mean scattering lengths in units  $\beta_3, \beta_4$ . The quantity  $\bar{a}/\beta_3$  grows to minus infinity for small  $\rho$ , indicating the increasing dominance of the  $-1/r^3$  tail. It rapidly approaches zero when  $\rho$  grows larger than unity, indicating a more and more decreasing influence of the  $-1/r^3$  tail and a more and more growing contribution of the  $-1/r^4$  tail. In contrast, the quantity  $\bar{a}/\beta_4$  goes to zero for small  $\rho$ , indicating a negligible contribution of the  $-1/r^4$  tail. This might be somewhat counterintuitive, but we remind the reader that small  $\rho$  means small  $\beta_3$  means large  $\beta_4$ , describing a relative dominance of the van der Waals contribution. Thus, a mean scattering length on the  $\beta_4$  scale in this limit is of no weight compared to the  $\beta_3$  scale, and thus should vanish. Quantitatively speaking,

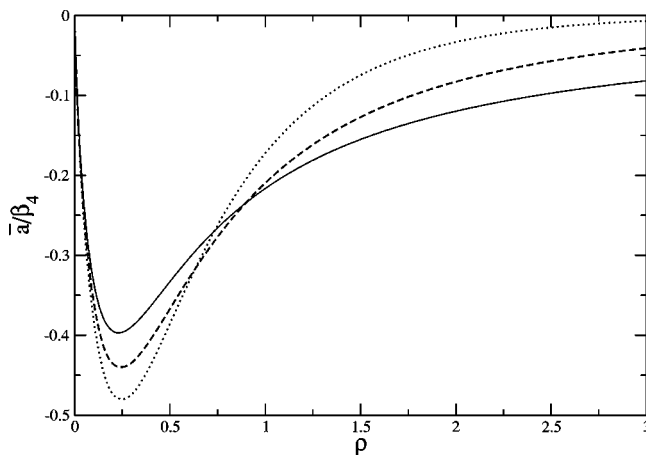


FIG. 11. Mean scattering length on  $\beta_4$  scale. Shimizu's potential (21) (full line), rational approximation (28) (dashed line), and arctan formula (29) (dotted line).

$$\frac{\bar{a}}{\beta_4} = \frac{\bar{a}}{\beta_3} \rho, \quad (36)$$

and this vanishes, as  $\rho \rightarrow 0$ .

For large  $\rho$ , we find the reverse situation. Figure 11 shows that  $\bar{a}/\beta_4$  tends to zero, but its value is always larger than the corresponding value of  $\bar{a}/\beta_3$ . Experimental [7,8] and theoretical (e.g., [6]) investigations of the quantum reflection probabilities suggest that the nonretarded van der Waals part of the potential is important only for high energies well away from threshold when  $\rho > 1$ . In this context it may seem surprising that the scattering lengths are negative for all  $\rho$  values. This shows that the influence of the nonretarded van der Waals potential on the phase of the quantum reflection amplitude is not negligible at threshold for any value of  $\rho$ .

#### IV. SUMMARY AND CONCLUSION

For three different model potentials for the Casimir-van der Waals interaction, we have calculated the phase of the quantum reflection amplitude and the associated space shifts for a narrow momentum distributed wave packet that is quantum reflected at the given potentials. We used a scaling theory that was invented especially for these types of inhomogeneous potentials, and examined the behavior of a quantum reflected atom depending on the critical parameter  $\rho$ . In analyzing the behavior of the reflected atom, we focused especially on the transition region in the vicinity of  $\rho \approx 1$ , where the intrinsic length scales change dominance. For  $\rho < 1$ , the  $-1/r^3$  tail shows more dominant behavior, where for  $\rho > 1$  the  $-1/r^4$  tail is dominant for quantum reflection. This behavior, deducible from simple scaling arguments, is confirmed by the numerical results for the phase of the quantum reflection amplitude. The strong influence of the van der Waals regime is mirrored in the phase by characteristic maxima, which indicate negative space shifts over a wide range of energy, corresponding to large time delays of the reflected atom for small velocities. For  $\rho > 1$  the highly retarded  $-1/r^4$  tail is more dominant. The characteristic van der Waals maximum flattens more and more, indicating a loss of the influence of the  $-1/r^3$  potential, which is more and more confined to very small velocities of the atom. Nevertheless, it is surprising, that the influence of the short ranged  $-1/r^3$  part of the potential persists at very small incident energies. One might expect that especially particles with incident energy just above threshold would experience only the long ranged  $-1/r^4$  part of the potential, because they are reflected before entering the short ranged region. But, as the foregoing examination has shown, the presence of a full Casimir-van der Waals interaction is more than a composition of its limiting regimes.

For larger velocities, the atom experiences a positive space shift, implying a time gain compared to a free moving atom. Recalling the results given in [10] for powers  $\alpha = (3, 4)$ , we clearly see that a Casimir-van der Waals interaction lies between these two cases. Which of the intrinsic scales is dominant depends strongly on the atomic properties.

By comparing the behavior of the mean scattering length of all three model potentials, we were able to work out the

most distinct differences between the three models, which are shown most clearly in this quantity. The phases of the reflection amplitude, i.e., the time and space shifts involved in the quantum reflection process, are a more sensitive test of the potential shape than the reflection probabilities.

#### ACKNOWLEDGMENT

We thank the Deutsche Forschungsgemeinschaft for supporting this work (Grant No. Az: Fr 591/12-1).

- 
- [1] R. Côté, H. Friedrich, and J. Trost, Phys. Rev. A **56**, 1781 (1997).
  - [2] M. J. Moritz, Ch. Eltschka, and H. Friedrich, Phys. Rev. A **63**, 042102 (2001).
  - [3] H. Friedrich, G. Jacoby, and C. G. Meister, Phys. Rev. A **65**, 032902 (2002).
  - [4] G. Jacoby and H. Friedrich, J. Phys. B **35**, 4839 (2002).
  - [5] B. Segev, R. Côté, and M. G. Raizen, Phys. Rev. A **56**, R3350 (1997).
  - [6] X. W. Halliwell, H. Friedrich, S. T. Gibson, and K. G. H. Baldwin, Opt. Commun. **224**, 89 (2003).
  - [7] F. Shimizu, Phys. Rev. Lett. **86**, 6 (2001).
  - [8] V. Druzhinina and M. DeKieviet, Phys. Rev. Lett. **91**, 193202 (2003).
  - [9] H. Friedrich and J. Trost, Phys. Rep. (to be published).
  - [10] H. Friedrich and A. Jurisch, Phys. Rev. Lett. **92**, 10302 (2004).
  - [11] E. P. Wigner, Phys. Rev. **98**, 1 (1955).
  - [12] A. Mody, M. Haggerty, J. M. Doyle, and E. J. Heller, Phys. Rev. B **64**, 085418 (2001).
  - [13] G. F. Gribakin and V. V. Flambaum, Phys. Rev. A **48**, 1 (1993).
  - [14] H. B. G. Casimir and D. Polder, Phys. Rev. **73**, 360 (1948).
  - [15] P. Kharchenko, J. F. Babb, and A. Dalgarno, Phys. Rev. A **55**, 3566 (1997).
  - [16] Y. Tikochinsky and L. Spruch, Phys. Rev. A **48**, 4223 (1993).
  - [17] Z.-C. Yan, A. Dalgarno, and J. F. Babb, Phys. Rev. A **56**, 2882 (1997).
  - [18] Z.-C. Yan and J. F. Babb, Phys. Rev. A **58**, 1530 (1998).
  - [19] M. Marinescu, A. Dalgarno, and J. F. Babb, Phys. Rev. A **55**, 1530 (1997).
  - [20] G. Feinberg and J. Sucher, Phys. Rev. A **2**, 6 (1970).
  - [21] B. Holstein, Am. J. Phys. **69**, 441 (2001).
  - [22] A. D. Polyinin and V. F. Zaitsev, *Handbuch der Linearen Differentialgleichungen* (Spektrum Akademie Verlag, Heidelberg, 1996), p. 46.